Applied Physics Letters

RESEARCH ARTICLE | MARCH 20 2023

Flexible self-powered DUV photodetectors with high responsivity utilizing Ga_2O_3/NiO heterostructure on buffered Hastelloy substrates

Xiao Tang; Yi Lu; Rongyu Lin; ... et. al

Appl. Phys. Lett. 122, 121101 (2023)
https://doi.org/10.1063/5.0146030

Applied Physics Letters ARTICLE scitation.org/journal/apl

Flexible self-powered DUV photodetectors with high responsivity utilizing Ga_2O_3/NiO heterostructure on buffered Hastelloy substrates

Cite as: Appl. Phys. Lett. **122**, 121101 (2023); doi: 10.1063/5.0146030
Submitted: 9 February 2023 · Accepted: 27 February 2023 ·
Published Online: 20 March 2023

Xiao Tang,[1] Yi Lu,[1] Rongyu Lin,[1] Che-Hao Liao,[1] Yue Zhao,[2] Kuang-Hui Li,[1] Na Xiao,[1] Haicheng Cao,[1] Wedyan Babatain,[1] and Xiaohang Li[1,a)]

AFFILIATIONS

[1]Computer, Electrical, and Mathematical Science and Engineering Division (CEMSE), King Abdullah University of Science and Technology (KAUST), Thuwal 23955-6900, Saudi Arabia
[2]School of Electronic Information and Electrical Engineering, Shanghai Jiao Tong University, Shanghai 200240, China

[a)]Author to whom correspondence should be addressed: Xiaohang.Li@kaust.edu.sa

ABSTRACT

In this research, β-Ga_2O_3/NiO heterostructures were grown directly on CeO_2 buffered Hastelloy flexible substrates. With pulsed laser deposition under high temperatures, as-grown β-Ga_2O_3 and NiO thin films have a preferred out-of-plane orientation along the $\langle -201 \rangle$ and $\langle 111 \rangle$ directions. This is due to the ideal epitaxial ability of the CeO_2 buffer layer, which serves as a perfect template for the epitaxial growth of single-oriented NiO and β-Ga_2O_3 by creating a constant gradient from CeO_2 (2.7 Å along $\langle 001 \rangle$) to NiO (2.9 Å along $\langle 110 \rangle$), and eventually to β-Ga_2O_3 (3.04 Å along $\langle 010 \rangle$). The Hastelloy substrates endow photodetectors with good deformability and mechanical robustness. Moreover, owing to the type-II band alignment of β-Ga_2O_3/NiO heterostructures, the photodetectors have a good photocurrent at zero bias under 284 nm of light illumination. In addition, the photocurrent is significantly higher than when using an analogous heterostructure (as described in some previous reports), because the β-Ga_2O_3 and NiO thin films are crystalized along a single orientation with fewer defects.

In recent years, β-Ga_2O_3 has attracted significant interest due to its ultra-wide bandgap (~4.9 eV), high breakdown electric field (~9 MV/cm), excellent thermal stability, and high absorption coefficient for deep ultraviolet (DUV) light.[1,2] Because of these unique properties, β-Ga_2O_3 is considered one of the best candidates for photodetector (PD) applications. However, to ensure that devices based on β-Ga_2O_3 are reliable and achieve high performance, the density of defects and dislocations in the β-Ga_2O_3 material must be limited. Therefore, β-Ga_2O_3 should be crystalized with a single orientation.[3,4] To realize the application of these photodetectors in the emerging fields of wearable and foldable electronics, such single-oriented β-Ga_2O_3 thin films are desired to be deposited on flexible substrates.[5] Until now, most of the reported single-oriented DUV photodetectors (PDs) based on β-Ga_2O_3 were fabricated on rigid substrates without any mechanical flexibility.[4,6,7] We notice that recently Chen *et al.* and Lu *et al.* both successfully synthesized β-Ga_2O_3 flexible PDs with excellent performances by using mica as the template.[8–10] In their work, they directly utilized the lattice structure of mica for epitaxial growth of β-Ga_2O_3.

Here, we report on the epitaxial growth of single-oriented β-Ga_2O_3 on a buffered Hastelloy flexible substrate. Different from mica, the Hastelloy substrate as a metallic material has much higher tensile strength; hence, it might be more promising in actual flexibility-required applications.[11,12] However, due to its polycrystalline nature with no preferred orientation, it cannot directly serve as an epitaxial template.

To solve this issue, the Hastelloy substrate is functionalized with single-oriented multi-buffer layers by using the ion-beam assisted deposition (IBAD) technique to meet the crystalline requirements for the epitaxy of β-Ga_2O_3. On the other hand, the energy supply systems of conventional flexible devices rely on external batteries, resulting in reduced portability and comfort of the products.[13] Hence, building flexible devices that operate without a power supply (i.e., self-powered) is essential. Previous reports have demonstrated that Ga_2O_3 photodetectors can operate in a self-powered mode when constructed with NiO to form a type-II p–n junction.[14,15] Inspired by their work, we report the direct epitaxial growth of the

single-oriented β-Ga_2O_3/NiO heterostructure on the buffered Hastelloy flexible substrate.

To realize the formation of a high-quality CeO_2 (001) layer, the Hastelloy substrate (10 mm width and 50 μm thickness) was initially coated successively with Al_2O_3 (80 nm) and Y_2O_3 (20 nm) layers using reactive RF sputtering. Subsequently, it was coated with MgO (5 nm) and $LaMnO_3$ (20 nm) using ion-beam assisted deposition (IBAD) and magnetron sputtering techniques, respectively. Here, Al_2O_3/Y_2O_3 served as the planarization layer, while $MgO/LaMnO_3$ served as the seed layer for CeO_2 growth. Then, 200 nm of the CeO_2 (001) buffer layer was grown using pulsed laser deposition (PLD) to finalize the functionalization of the Hastelloy substrate. On top of the CeO_2 layer, an n-type β-Ga_2O_3 (silicon-doped 1 wt. %)/p-type NiO (lithium-doped 1 wt. %) heterostructure was successively grown using PLD with a laser pulse frequency of 5 Hz and an energy per pulse of 450 mJ. During deposition, the substrate temperature and oxygen partial pressure were, respectively, set to 400 °C and 200 mTorr for the NiO layer and 640 °C and 5 mTorr for the Ga_2O_3 layer.

A cross-sectional transmittance electron microscopy (TEM) image and energy dispersive X-ray spectrum (EDX) for the β-Ga_2O_3/NiO/CeO_2/$LaMnO_3$/MgO/Y_2O_3/Al_2O_3/Hastelloy stacked structure are, respectively, depicted in Figs. 1(a) and 1(b). The EDX images indicate the formation of clear interfaces between each layer in the stacked structure. In particular, no element (Ga, Ni, or Ce) diffusion can be observed between the β-Ga_2O_3, NiO, and CeO_2 layers.

Figure 2(a) presents the XRD 2-theta patterns of the stacked structure, where a strong (002) peak together with a weak (111) peak can be observed for CeO_2. Here, (002) is the preferred orientation, and (111) is the random orientation. Above CeO_2, the NiO layer only exhibits the preferred orientation along (111). The β-Ga_2O_3 layer is characterized by a series of diffraction peaks from the {−201} planes. Overall, the 2-theta patterns demonstrate an epitaxial relationship of β-Ga_2O_3 {−201}//NiO {111}//CeO_2 {001} for the β-Ga_2O_3/NiO/CeO_2 stacked structure, which can also be reflected from the FFT patterns in Fig. 1(c).

To elucidate the in-plane epitaxial relationship of the β-Ga_2O_3/NiO/CeO_2 stacked structure, we also measured the phi-scan XRD pattern on (111) reflections of CeO_2, (001) reflections of NiO, and (−401) reflections of β-Ga_2O_3, as shown in Fig. 2(b). The phi-scans

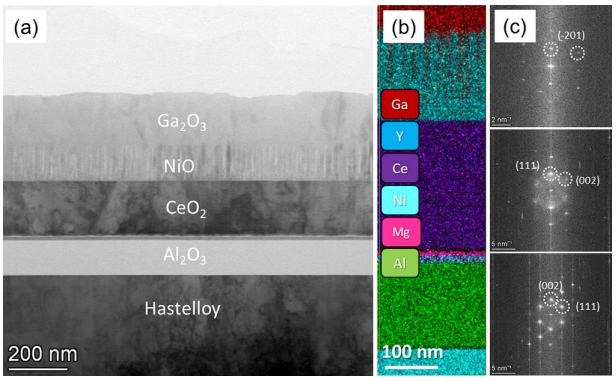

FIG. 1. (a) Cross-sectional TEM image; (b) corresponding EDX mapping of the stacked structure; (c) fast Fourier transform (FFT) pattern for the layers of β-Ga_2O_3, NiO, and CeO_2 (from top to bottom).

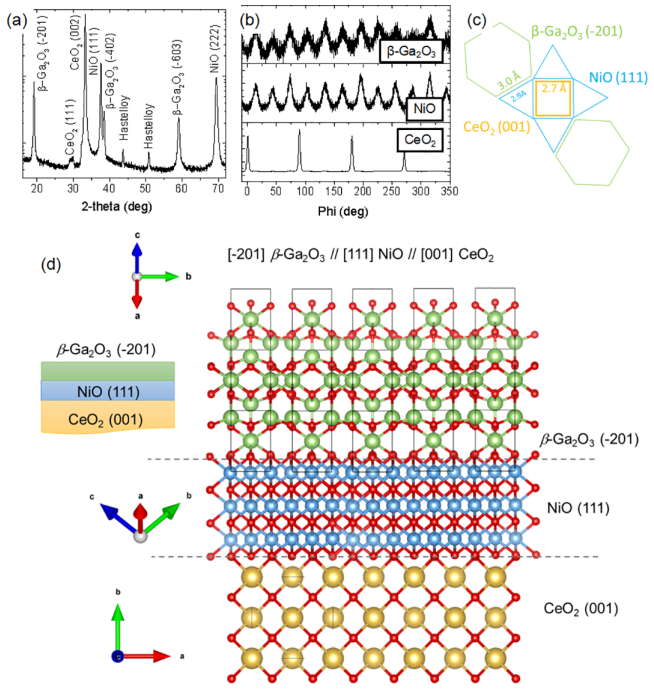

FIG. 2. (a) 2-theta XRD spectra measured on the β-Ga_2O_3/NiO/CeO_2/$LaMnO_3$/MgO/Y_2O_3/Al_2O_3/Hastelloy stacked structure; (b) phi-scan for the layers of β-Ga_2O_3, NiO, and CeO_2 (from top to bottom); (c) simplified scheme of the epitaxial relationship between the β-Ga_2O_3 (−201), NiO (111), and CeO_2 (001) planes; (d) atomic arrangement model of the β-Ga_2O_3 (−201)/NiO (111)/CeO_2 (001) stacked structure.

for CeO_2 exhibited four distinct peaks with an interval of 90°, indicating a typical in-plane cubic fourfold symmetry. The phi-scans for both NiO and β-Ga_2O_3 indicated 12 peaks appearing at the same positions with an interval of 30°. Interestingly, we did not observe "cube-on-cube" in-plane epitaxy when NiO was grown on CeO_2 (001). This is due to the large mismatch (55%) between the lattice constants along NiO (001) and CeO_2 (001), which were 4.2 and 2.7 Å, respectively.[16,17] In contrast, the lattice constant for NiO along (011) was 2.9 Å, resulting in a small lattice mismatch of 7% with the lattice constant for CeO_2 along (001).[17] As a result, NiO (111), instead of (001), was epitaxially grown on the CeO_2 (001). It is known that NiO (111) has threefold symmetry; therefore, the appearance of the 12 peaks in the phi-scan indicates the formation of four NiO (111) domains with a rotation angle of 90° between them. For β-Ga_2O_3, the lattice constant along [010] was 3.04 Å, resulting in a lattice mismatch between the NiO [110] and the β-Ga_2O_3 [010] of only 3.4%.[4,17] Hence, β-Ga_2O_3 (−201) can be readily grown on NiO (111) with two domains rotated by an angle of 90°. The results also revealed that NiO (111) serves as a buffer layer by providing a lattice gradient from CeO_2 (001) to β-Ga_2O_3 (−201). Since the β-Ga_2O_3 (−201) plane has sixfold symmetry, the 12 peaks in the phi-scan indicated the formation of two β-Ga_2O_3 (−201) domains with a rotation angle of 90° between them. A simplified scheme for the epitaxial relationship between the β-Ga_2O_3 (−201), NiO (111), and CeO_2 (001) planes and an atomic arrangement model for the whole β-Ga_2O_3 (−201)/NiO (111)/CeO_2 (001) stacked structure are illustrated in Figs. 2(c) and 2(d), respectively.

Following thin film deposition, a part of β-Ga_2O_3 was completely etched using BCl_3. Then, the sample was fabricated into photodetectors by depositing Ti/Au (R = 120 μm) and Ni/Au (R = 150 μm) concentric rings as the electrodes on top of β-Ga_2O_3 and NiO, respectively. It should be noted that a 2 μm gap was incorporated between the β-Ga_2O_3 part and the Ni/Au electrode to avoid any direct contact. The flexible photodetectors and geometry (inset) are shown in Fig. 3(a). The current–voltage (I–V) curves of the photodetectors in the dark conditions and under 284 nm light illumination with a power density of 15 $\mu W/cm^2$ are depicted in Fig. 3(b). The photodetector exhibited clear rectifying I − V characteristics and a photocurrent above 3 nA at zero bias under light illumination. The photoresponsivity at zero bias was calculated as 600 mA/W using

$$R = \frac{I_{photo} - I_{dark}}{D \times S}, \quad (1)$$

where R, I_{photo}, I_{dark}, D, and S are the photoresponsivity, photocurrent, dark current, light power density, and exposure area, respectively. The photocurrent as a function of the illumination light wavelength is shown in Fig. 3(c). The spectrum was characterized by a broad peak from 350 to 200 nm, centered at 284 nm. Such broad detectivity can be ascribed to two collective effects. The first is from the bandgap (4.8 eV) of β-Ga_2O_3 relating to the electronic transition from O 2p occupied states to Ga 5s unoccupied states. The second is the bandgap (3.6 eV) of NiO relating to the electronic transitions from the occupied O 2p states hybridized with Ni 3d characteristics to the unoccupied Ni 3d state.[21] Based on the spectrum, a rejection ratio (R284/R450 nm) of approximately 3×10^3 was obtained, suggesting high spectral selectivity. The time-dependent photoresponse (I − t) is shown in Fig. 3(d), which was achieved by turning the 284 nm illuminating light on and off periodically at zero bias. The measurement was performed under three conditions: flat, bending, and flat after a fatigue test of 2000 bending cycles. Here, the bending condition was achieved by pasting the flexible sample on semicircular cylinder molds with a radius of 10 mm, as shown in Fig. 3(e). Furthermore, the fatigue test was conducted by automatically stretching and compressing the sample using a homemade machine. The results indicated that the flexible photodetector has a fast response when turning the UV illumination on and off. Since the sample was largely unaffected by the bending and fatigue tests, it can be considered to have high mechanical robustness. The photocurrent response for a single cycle of the flexible photodetector is shown in Fig. 3(f). By applying bi-exponential fitting, the response time (τ_r) and the decay time (τ_d) were estimated as 0.14 and 0.49 s, respectively.

To obtain a more fundamental understanding of the self-powered photoelectrical performances of the devices, the β-Ga_2O_3/NiO heterostructure was also subjected to high-resolution x-ray photoelectron spectroscopy (HR-XPS) measurements to investigate the band alignment, as shown in Figs. 4(a)–4(c). By applying Eqs. (2) and (3), the offsets of the valence band VBO (ΔEv) and the conduction band CBO (ΔE_C) were obtained,

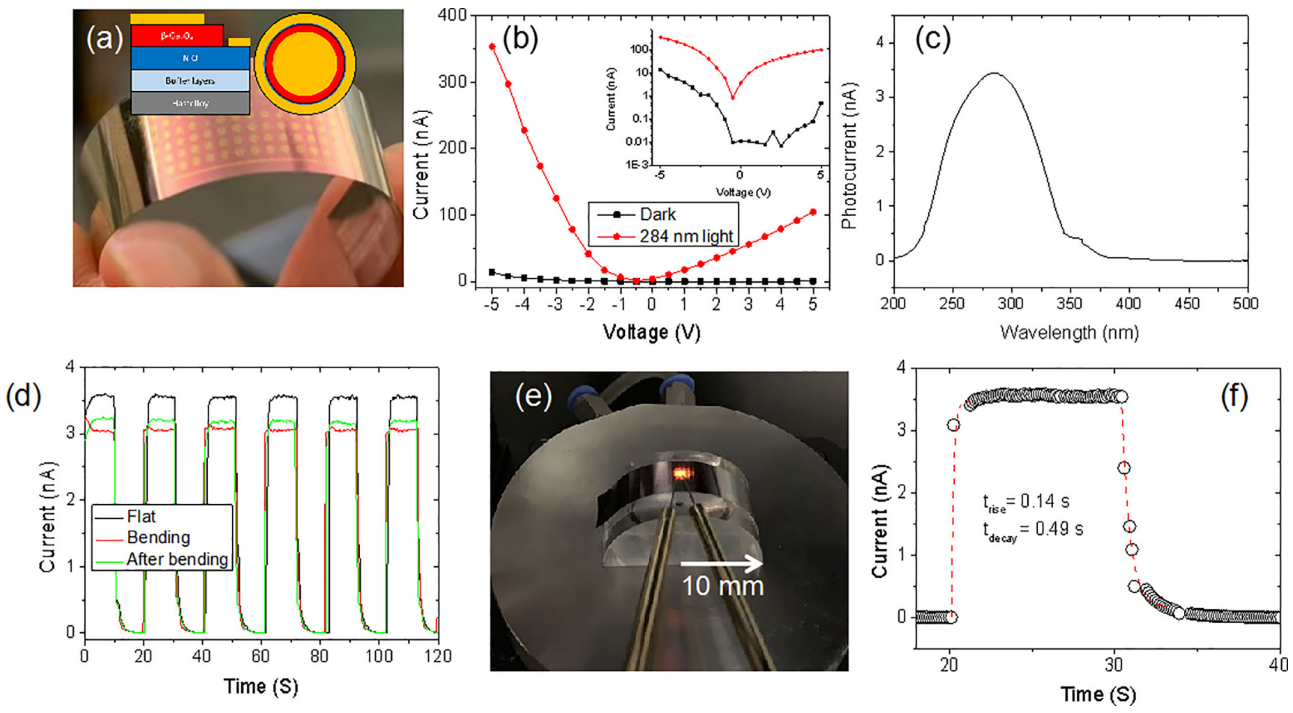

FIG. 3. (a) Picture of the flexible photodetectors and the geometry (inset); (b) I–V curve in linear and log scales (inset) measured on the photodetector in both a dark condition and under 284 nm of light illumination; (c) wavelength-dependent responsivity of the sample; (d) time-dependent photoresponse curves measured on the sample under 284 nm light illumination that turned on/off periodically at 10 s intervals for three conditions: flat, bending, and after the fatigue test; (e) picture of the sample under bending; (f) photocurrent response for a single on/off cycle.

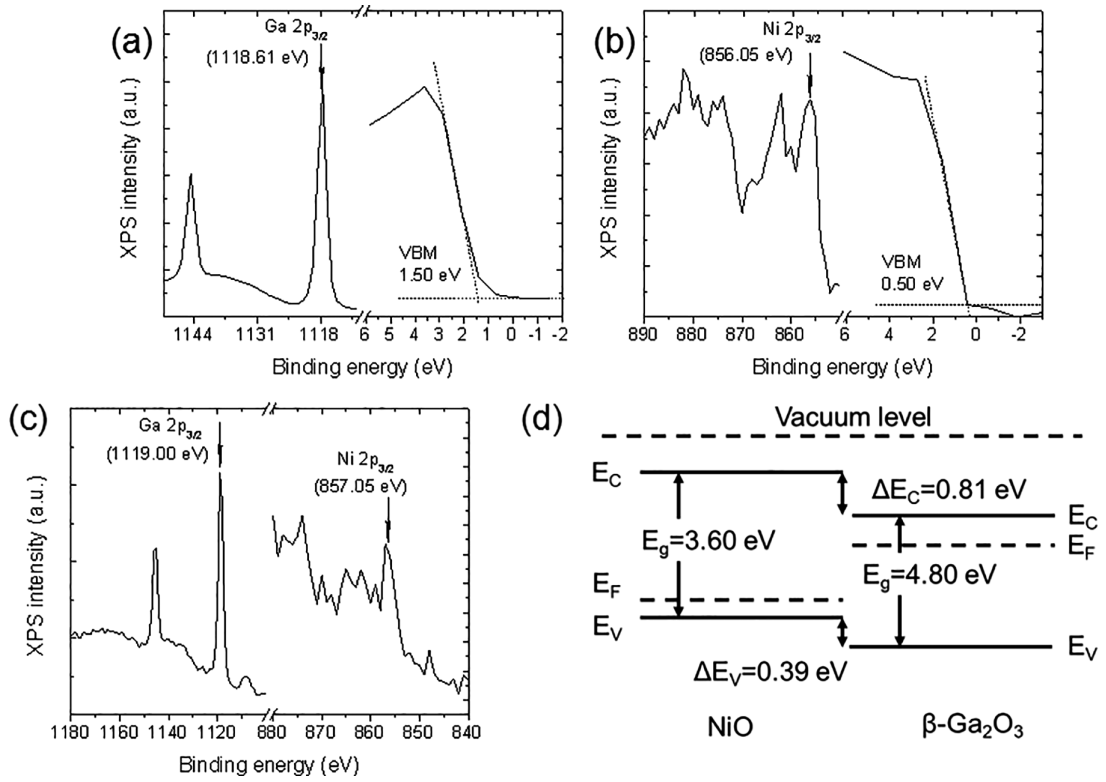

FIG. 4. (a) XPS spectra of Ga 2p core levels and the valence band from the β-Ga_2O_3 layer; (b) XPS spectra of Ni 2p core levels and the valence band from the NiO layer; (c) XPS spectra of Ga 2p and Ni 2p core levels for the β-Ga_2O_3/NiO heterostructure; (d) schematic representation of the band alignment at the β-Ga_2O_3/NiO interface.

$$\Delta E_V = (E^{\beta-}_{Ga^2O_3\,2p}{}^{Ga} - E^{\beta-}_{Ga^2O_3\,VBM}) - (E^{NiO}_{3d} - E^{NiO}_{VBM}) + (E^{\beta-}_{Ga^2O_3\,Ni\,3d}{}^{/NiO} - E^{\beta-}_{Ga^2O_3\,Ga\,2p}{}^{/NiO}), \quad (2)$$

$$\Delta E_C = (E^{NiO}_g - E^{\beta-}_{Ga^2O_3 g}) - \Delta E_V. \quad (3)$$

Here, $E^{\beta-}_{Ga^2O_3\,2p}{}^{Ga}$, $E^{\beta-}_{Ga^2O_3\,VBM}$, E^{NiO}_{3d}, and E^{NiO}_{VBM} are the core levels and the valence band maximum (VBM) for β-Ga_2O_3 and NiO, respectively; $E^{\beta-}_{Ga^2O_3\,Ni\,3d}{}^{/NiO}$ and $E^{\beta-}_{Ga^2O_3\,Ga\,2p}{}^{/NiO}$ are the corresponding values obtained on the β-Ga_2O_3/NiO heterostructure; and E^{NiO}_g and $E^{\beta-}_{Ga^2O_3 g}$ are the optical band gaps of NiO and β-Ga_2O_3, respectively.[18]

The core levels and the valence band maximum (VBM) were obtained from the XPS results, as shown in Figs. 4(a)–4(c). For NiO, the binding energy of Ni $2p_{3/2}$ and the VBM were 856.05 and 0.50 eV, respectively. For β-Ga_2O_3, the binding energy of Ga $2p_{3/2}$ and the VBM were 1118.61 and 1.50 eV, respectively. Accordingly, the separation energy between the core level and the VBM for NiO and β-Ga_2O_3 were 855.55 and 1117.11 eV, respectively.

For the β-Ga_2O_3/NiO heterostructure, the binding energies of Ni $2p_{3/2}$ and Ga $2p_{3/2}$ were determined as 857.05 and 1119.00 eV, respectively. Then, the energy discrepancy between the Ga $2p_{3/2}$ and Ni $2p_{3/2}$ core levels was calculated as 261.95 eV. In general, the optical bandgap for NiO and β-Ga_2O_3 is obtained by using UV−vis measurements. However, in this research, because the Hastelloy substrate is not transparent, UV-Vis measurements were not straightforward to perform. Therefore, the bandgap values for NiO and β-Ga_2O_3 were obtained directly from previous reports as 4.80 and 3.60 eV, respectively.[19,20] Based on these results, ΔE_V and ΔE_C were calculated as 0.39 and 0.81 eV, respectively.

Based on the previously determined values, a type-II band alignment for the β-Ga_2O_3/NiO heterostructure was estimated, as shown in Fig. 4(d). In such a β-Ga_2O_3/NiO heterostructure, NiO and β-Ga_2O_3 have different Femi energy levels. To reach a unified Femi energy level in thermal equilibrium, the electrons in the n-type β-Ga_2O_3 layer move to the NiO film side, while the holes in the p-type NiO layer move in the opposite direction. As a result, downward and upward bending occurs at energy levels near the p-type NiO and n-type β-Ga_2O_3 surfaces, respectively. Meanwhile, a built-in electric field from β-Ga_2O_3 to NiO is created at the β-Ga_2O_3/NiO interface. In dark conditions, the built-in potential can provide a small number of electrons and holes in the heterostructure with flowing mobility, resulting in a low dark current, even under zero-bias voltage. In contrast, a large number of electron-hole pairs is created when the heterostructure is illuminated by DUV light. Moreover, increased carrier density at the interface can narrow the depletion region and decrease the barrier height. As a result, the current is significantly enhanced when the device is under light illumination.

To conclude, the developed flexible self-powered photodetectors based on the β-Ga_2O_3/NiO type-II heterostructure exhibit good deformability and mechanical robustness while achieving superior

TABLE I. Comparison of the flexible self-powered β-Ga_2O_3/NiO PD described in this work with previously reported flexible Ga_2O_3/NiO PDs.[14,15]

Crystal quality (β-Ga_2O_3/NiO)	Responsivity (mA/W at 0 V)	Response time (rise/decay) (s)	Light power density ($\mu W/cm^2$)	References
Single-orientation/random orientation	1.78	0.012/0.08	270	14
Amorphous/single-orientation	0.05	0.34/3.65	100	15
Single-orientation/single-orientation	600	0.49/0.14	15	This work

photo responsivity and similar response speed compared to devices that use the analogous heterostructure described in some previous reports.[9,10] The key parameters include the crystal quality of Ga_2O_3 and NiO, responsivity, and response speeds, and the illuminating conditions described in this work (and the other two reports) are summarized in Table I. In the other reports, the photodetectors were illuminated by a 254 nm single wavelength ultraviolet (DUV) lamp, while the light source in our research was a xenon lamp that incorporated a monochrometer. This meant that the power density (15 $\mu W/cm^2$) was much smaller compared to the other reports (at least 100 and 300 $\mu W/cm^2$). It is known that the responsivity decreases with applied light intensity due to the self-heating effect induced by strong light illumination. Hence, the illuminating power difference could be a reason for the high responsivity obtained in our research. More importantly, we believe that the high responsivity can also be attributed to the ideal epitaxial ability of the CeO_2 buffer layer, which serves as a perfect template for the epitaxial growth of single-oriented NiO and β-Ga_2O_3. This is achieved by creating a constant gradient from CeO_2 (2.7 Å along ⟨001⟩) to NiO (2.9 Å along ⟨110⟩) and eventually to β-Ga_2O_3 (3.04 Å along ⟨010⟩). In contrast, the heterostructures in the previous reports used either amorphous or randomly oriented Ga_2O_3/NiO thin films, in which a large number of trap states can accumulate on the defects and oxygen vacancies.[1,4,22] When illuminated by light, excited electrons can be easily captured by such trap states. Consequently, this causes amorphous/randomly oriented Ga_2O_3/NiO thin films to exhibit much lower photo responsivity compared to the mono-oriented counterparts described in our research. In summation, we provide an ideal flexible platform for *in situ* growing of a single-oriented β-Ga_2O_3/NiO heterostructure, which is promising for making flexible self-powered DUV photodetectors.

The authors would like to thank the KAUST Baseline Fund via No. BAS/1/1664-01-01, the Competitive Research Grant via Nos. URF/1/3437-01-01 and URF/1/3771-01-01, and the GCC Research Council via Grant No. REP/1/3189-01-01 for their support.

AUTHOR DECLARATIONS

Conflict of Interest

The authors have no conflicts to disclose.

Author Contributions

Xiao Tang: Conceptualization (equal); Data curation (equal); Formal analysis (equal); Writing – original draft (equal); Writing – review & editing (equal). **Xiaohang Li:** Project administration (equal); Supervision (equal). **Yi Lu:** Data curation (equal); Investigation (equal); Methodology (equal). **Rongyu Lin:** Software (equal). **Che-Hao Liao:** Investigation (equal). **Yue Zhao:** Investigation (equal); Resources (equal). **Kuang-Hui Li:** Investigation (equal). **Na Xiao:** Formal analysis (equal). **Haicheng Cao:** Investigation (equal). **Wedyan H. Babatain:** Resources (equal).

DATA AVAILABILITY

The data that support the findings of this study are available from the corresponding author upon reasonable request.

REFERENCES

[1]H. Peelaers and C. G. Van de Walle, Phys. Status Solidi B **252**, 828 (2015).
[2]D. Guo, Q. Guo, Z. Chen, Z. Wu, P. Li, and W. Tang, Mater. Today Phys. **11**, 100157 (2019).
[3]Q. Wang, J. Chen, P. Huang, M. Lia, Y. Lu, K. P. Homewood, G. Chang, H. Chen, and Y. He, Appl. Surf. Sci. **489**, 101 (2019).
[4]X. Tang, K.-H. Li, C.-H. Liao, D. Zheng, C. Liu, R. Lin, N. Xiao, S. Krishna, J. Tauboada, and X. Li, J. Mater. Chem. C **9**, 17542 (2021).
[5]I. M. Asuo, P. Fourmont, I. Ka, D. Gedamu, S. Bouzidi, A. Pignolet, R. Nechache, and G. S. Cloutier, Small **15**(1), e1804150 (2019).
[6]Z. Feng, A. U. Bhuiyan, M. R. Karim, and H. Zhao, Appl. Phys. Lett. **114**, 250601 (2019).
[7]X. Tang, K.-H. Li, C.-H. Liao, J. M. T. Vasquez, C. Wang, N. Xiao, and X. Li, J. Eur. Ceram. Soc. **42**, 175 (2022).
[8]W.-H. Chen, C.-H. Ma, S.-H. Hsieh, Y.-H. Lai, Y.-C. Kuo, C.-H. Chen, S.-P. Chang, S.-J. Chang, R.-H. Horng, and Y.-H. Chu, ACS Appl. Electron. Mater. **4**, 3099 (2022).
[9]Y. Lu, S. Krishna, X. Tang, W. Babatain, M. B. Hassine, C.-H. Liao, N. Xiao, Z. Liu, and X. Li, ACS Appl. Mater. Interfaces **14**, 34844 (2022).
[10]Y. Lu, S. Krishna, C.-H. Liao, Z. Yang, M. Kumar, Z. Liu, X. Tang, N. Xiao, M. B. Hassine, S. T. Thoroddsen, and X. Li, ACS Appl. Mater. Interfaces **14**, 47922 (2022).
[11]S. Habelitz, G. Carl, C. Rüssel, S. Thiel, U. Gerth, J.-D. Schnapp, A. Jordanov, and H. Knake, J. Non-Cryst. Solids **220**, 291 (1997).
[12]K. K. Mehta, P. Mukhopadhyay, R. K. Mandal, and A. K. Singh, Metall. Mater. Trans. A **45**, 3493 (2014).
[13]E. Bihar, D. Corzo, T. C. Hidalgo, D. Rosas-Villalva, K. N. Salama, S. Inal, and D. Baran, Adv. Mater. Technol. **5**, 2000226 (2020).
[14]Y. Wang, C. Wu, D. Guo, P. Li, S. Wang, A. Liu, C. Li, F. Wu, and W. Tang, ACS Appl. Electron. Mater. **2**, 2032 (2020).
[15]J. Yu, M. Yu, Z. Wang, L. Yuan, Y. Huang, L. Zhang, Y. Zhang, and R. Jia, IEEE Trans. Electron. Devices **67**, 3199 (2020).
[16]X. Tang, K.-H. Li, Y. Zhao, Y. Sui, H. Liang, Z. Liu, C.-H. Liao, W. Babatain, R. Lin, C. Wang, Y. Lu, F. S. Alqatari, Z. Mei, W. Tang, and X. Li, ACS Appl. Mater. Interfaces **14**, 1304 (2022).
[17]D. Majumder, I. Chakraborty, K. Mandal, and S. Roy, ACS Omega **4**, 4243 (2019).
[18]K.-H. Li, N. Alfaraj, C.-H. Kang, L. Braic, M. N. Hedhili, Z. Guo, T. K. Ng, and B. S. Ooi, ACS Appl. Mater. Interfaces **11**, 35095 (2019); E. A. Kraut, R. W. Grant, J. R. Waldrop, and S. P. Kowalczyk, Phys. Rev. Lett. **44**, 1620 (1980).
[19]X.-Q. Zheng, H. Zhao, and P. X.-L. Feng, Appl. Phys. Lett. **120**, 040502 (2022).
[20]A. B. Kunz, J. Phys. C: Solid State Phys. **14**, L455 (1981).
[21]H. Gong, X. Chen, Y. Xu, Y. Chen, F. Ren, B. Liu, S. Gu, R. Zhang, and J. Ye, IEEE Trans. Electron Devices **67**, 3341 (2020).
[22]Z. Liu, Y. Zhi, S. Li, Y. Liu, X. Tang, Z. Yan, P. Li, X. Li, D. Guo, Z. Wu, and W. Tang, J. Phys. D: Appl. Phys. **53**, 085105 (2020).